Zitierweise: *Angew. Chem. Int. Ed.* **2020**, *59*, 21719–21727
Internationale Ausgabe: doi.org/10.1002/anie.202009520
Deutsche Ausgabe: doi.org/10.1002/ange.202009520

Phase Transformations

Quantification of High-Temperature Transition Al_2O_3 and Their Phase Transformations**

Libor Kovarik, Mark Bowden,* Amity Andersen, Nicholas R. Jaegers, Nancy Washton und János Szanyi*

Abstract: *High-temperature treatment of γ-Al_2O_3 can lead to a series of polymorphic transformations, including the formation of δ-Al_2O_3 and θ-Al_2O_3. Quantification of the microstructure in the range where δ- and θ-Al_2O_3 are formed represents a formidable challenge, as both phases accommodate a high degree of structural disorder. In this work, we explore the use of an XRD recursive-stacking formalism for the quantification of high-temperature transition aluminas. We formulate the recursive-stacking methodology for modelling of disorder in δ-Al_2O_3 and twinning in θ-Al_2O_3 and show that explicitly accounting for the disorder is necessary to reliably model the XRD patterns of high-temperature transition alumina. We also use the recursive stacking approach to study phase transformation during high-temperature (1050 °C) treatment. We show that the two different intergrowth modes of δ-Al_2O_3 have different transformation characteristics and that a significant portion of δ-Al_2O_3 is stabilized with θ-Al_2O_3 even after prolonged high-temperature exposures.*

Introduction

Transition aluminas represent an important group of materials that are used in a number of technological fields. For example, transition aluminas are prominently used as catalysts and catalytic supports.[1–3] In an effort to rationalize the attractive properties of transition aluminas, and ultimately understand how the properties can be tailored for specific catalytic applications, significant research efforts have focused on understanding the crystallography, structure and surfaces of transition aluminas.[4–7] For transition alumina derived from the heat treatment of boehmite, the microstructure is conventionally described in terms of γ-, δ- and θ-Al_2O_3. The microstructure consists of γ-Al_2O_3 if obtained from heat treatments below ≈700–800 °C.[4] At higher heat treatment temperatures, above 800 °C, the structure topotactically reorders to structural forms of δ- and θ-Al_2O_3.[4,8]

The formation and stability of transition alumina phases are actively studied topics. It is generally well established that the formation of δ-Al_2O_3 requires less thermal activation, while θ-Al_2O_3 is more stable and is the preferred type at higher temperatures of ≈950–1000 °C where kinetic factors play smaller roles.[4] Consequently, the formation of δ- and θ-Al_2O_3 has been conventionally expressed in terms of heat treatment temperature.[4,9] While this provides a useful conceptual view, it is now realized that such description may not satisfactorily capture the complexity of the evolving microstructures. Both δ-Al_2O_3 and θ-Al_2O_3 can coexist in a common microstructure over a broad temperature range[4] and, moreover, the evolving structures can encompass an intermediate state containing the bonding environment of both δ- and θ-Al_2O_3.[10] In addition, it has also been shown that the formation of δ-Al_2O_3 can be bypassed and θ-Al_2O_3 formed directly from γ-Al_2O_3. This has been demonstrated for transformation from γ-Al_2O_3 with a rod-like morphology derived from boehmite.[11] As both structures of δ- and θ-Al_2O_3 have a complex crystallography and accommodate a high degree of structural disorder,[4,10,12–14] reliable quantification and tracking of the microstructure as it evolves during phase transformations is the main limitation in advancing our understanding of high temperature transition aluminas.

Conventional XRD or NMR approaches that do not explicitly account for disorder are not well suited for structural analysis of these complex systems.[7,10,15] In order to address the stability and mechanism of transformations of high temperature transition aluminas, this work explores the possibility of adopting recursive stacking XRD quantification. The recursive stacking XRD techniques has been previously developed for analysis of planar disorder,[16] making it thus suitable for the analysis of the dominant disorders in δ/θ-Al_2O_3 microstructure. In δ-Al_2O_3, the disorder originates largely from the planar intergrowth of four δ_x-Al_2O_3 variants.[13,14] There are also other types of disorder present, such as porosity, domains, and points defects,[12] but these are not suited for recursive stacking formalism. In θ-Al_2O_3, there are two main types of superimposed structural disorders.[10] Only one of these has a planar character (twinning), and is thus suitable for analysis using recursive stacking. The use of recursive stacking has been previously applied for characterization/quantification of structural intergrowth in zeolites,[17] oxides,[18] twinned and disordered

[*] Dr. L. Kovarik, Dr. N. R. Jaegers, Dr. N. Washton, Dr. J. Szanyi
Institute for Integrated Catalysis, Pacific Northwest National Laboratory
P.O. Box 999, Richland, WA 99352 (USA)
E-Mail: libor.kovarik@pnnl.gov
Dr. M. Bowden, Dr. A. Andersen, Dr. N. Washton
Environmental Molecular Sciences Laboratory, Pacific Northwest National Laboratory
P.O. Box 999, Richland, WA 99352 (USA)
E-Mail: mark.bowden@pnnl.gov

[**] A previous version of this manuscript has been deposited on a preprint server (doi.org/10.26434/chemrxiv.12584783.v1).

Supporting information and the ORCID identification number(s) for the author(s) of this article can be found under: https://doi.org/10.1002/anie.202009520.

structures of SiC and kaolinite and other known planar defected structures.[19]

We develop a methodology for recursive stacking in δ-Al_2O_3 and θ-Al_2O_3 and demonstrate that explicitly accounting for this type of disorder is necessary to reliably model the XRD patterns of high temperature transition aluminas. The methodology is applied to study phase transformation in high temperature transition aluminas derived from boehmite, enabling us to describe the complexities in the evolution of δ- and θ-Al_2O_3 and their stabilities.

Results and Discussion

High-Temperature Transition Al_2O_3

We formulate the recursive stacking description of disorder in δ-Al_2O_3 and twinning in θ-Al_2O_3 based on crystallographic analysis of δ- and θ-Al_2O_3 provided in previous works.[10,13,14] According to this work, the high temperature microstructure can be conceptually described in terms δ-Al_2O_3 intergrowth, with two different intergrowth modes, and θ-Al_2O_3 with two superimposed types of structural disorder. A depiction of the structural components of high temperature transition Aluminas is shown in Figure 1.

In δ-Al_2O_3, there are two types of intergrowths. The first type is labeled as $\delta_{1,2}$-Al_2O_3, and as suggested by the notation, the intergrowth consists of δ_1- and δ_2-Al_2O_3 variants. The variants are structurally very similar but subtle differences can be identified based on the population of different subsets of Al sublattice vacant/octahedral/tetrahedral sites. The high degree of similarity enables considerable structural intergrowth. The second type of intergrowth is labeled as $\delta_{2,3,4}$-Al_2O_3, and originates from δ_2-, δ_3- and δ_4-Al_2O_3 variants. All three variants are based on an identical structural unit but stacked according to different translational and rotational operators. A detailed account of these intergrowth structures was provided by Kovarik et al.[14] Because of the planar nature of the intergrowths, the XRD recursive stacking approach provides an ideal method for microstructural characterization of planar intergrowth in δ-Al_2O_3 and can be applied to quantification in mixtures using Rietveld fitting of powder diffraction patterns.

The structure of θ-Al_2O_3 accommodates two superimposed types of disorder, including twinning and „2D-structural" disorder. Twinning is almost exclusively restricted to (100) as shown in Figure 1. It is often present in very high densities,[10,20] and thus it is an important component of θ-Al_2O_3 structure. Twinning represents a planar fault, and XRD recursive stacking approaches provide an ideal way of capturing and quantifying its extent.

On the other hand, 2D structural disorder does not have a planar character, and cannot be modeled with recursive stacking approaches. Other more generic approaches, such as Debye scattering would be appropriate to account for this disorder.[21] Given the current limitation of implementing 2D structural disorder, the present study treats θ-Al_2O_3 as an ideal structure of β-Ga_2O_3, which has 50% octahedral and 50% tetrahedral Ga^{3+} ions. This is an approximation of θ-Al_2O_3, which is expected to have 43%-48% of tetrahedral Al^{3+}.[10]

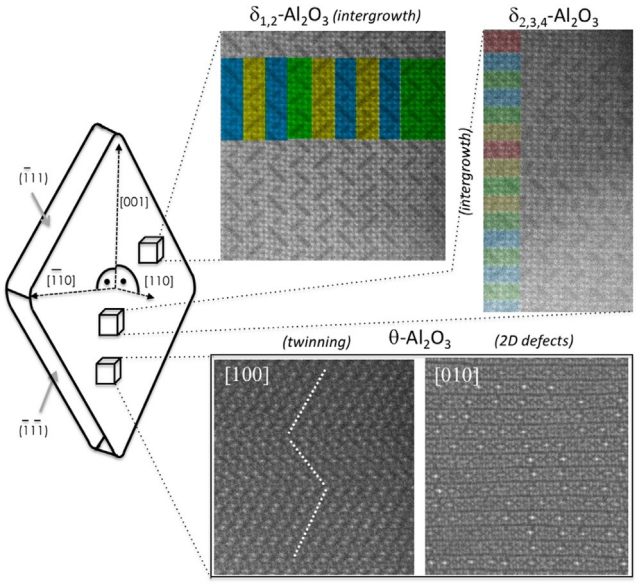

Figure 1. Schematic representation of the components of transition Alumina in δ/θ-Al_2O_3 stability region.

Methodology of Modelling Intergrowth/Twinning

Model of Intergrowth in $\delta_{1,2}$-Al_2O_3: Intergrowth in $\delta_{1,2}$-Al_2O_3 is formulated as a recursive stacking of four layers. As shown in Figure 2, two layers are derived from δ_1-Al_2O_3, and two layers are derived from δ_2-Al_2O_3. For the two layers derived from δ_1-Al_2O_3, each layer corresponds to half of the unit cell. For the two layers derived from δ_2-Al_2O_3, each represents a full unit cell of δ_2-Al_2O_3, but they are related by a 180° rotation, in order to accommodate the structure with δ_1-Al_2O_3 segments. As shown in Figure 2, the lattice correspondence between the layers from variants of δ_1-Al_2O_3 and δ_2-Al_2O_3 can be expresses as $[001]_{\delta1}//[010]_{\delta2}$ and $[010]_{\delta1}//[001]_{\delta2}$.

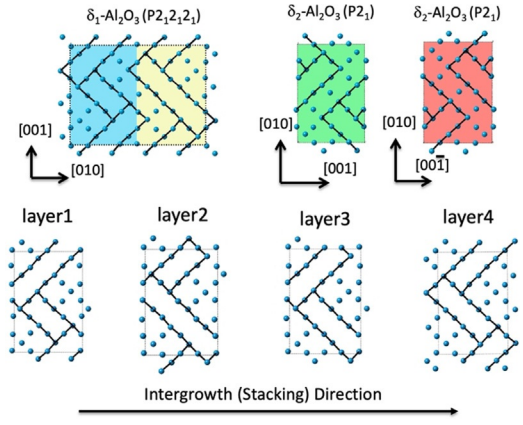

Figure 2. Formulation of structural intergrowth of δ_1-Al_2O_3 and δ_2-Al_2O_3. The structure is built by four layers, which represent the individual components of δ_1-Al_2O_3 and δ_2-Al_2O_3.

All four layers in the recursive stacking have been translationally aligned with respect to each other to meet the stacking constrains, and the recursive stacking Scheme itself does not require any additional translation offset perpendicular to the stacking direction. The rules for stacking of individual layers and creating intergrowth structures under the probability of occurrence for each variant are listed in Table S1. For example, layer 1, which represent δ_1-Al_2O_3 component, can only be followed by layer 2 (δ_1-Al_2O_3) or by layer 4 (δ_2-Al_2O_3). The proportion of δ_1-Al_2O_3 is controlled by probability value ($\delta_{1\%}$), and δ_2-Al_2O_3 by probability value $\delta_{2\%} = (100\text{-}\delta_{1\%})$.

Model of Intergrowth in $\delta_{2,3,4}$-Al_2O_3: Intergrowth in $\delta_{2,3,4}$-Al_2O_3 is formulated as a recursive stacking of eight layers, which differ only by their rotational and translation arrangement. The way the layers are related to the individual variants of δ_x-Al_2O is shown in Figure 3. Each layer represents a half-unit cell from either of the three variants of δ_x-Al_2O_3, as shown in Figure 3.

The rules for stacking of individual layers in the intergrowth is listed in Table S2. The sequence of layers for the individual variants in the intergrowth is defined by probability δ_x%. For example, δ_2-Al_2O_3 is obtained from stacking of layers 1→2, 2→1 or 3→4, 4→3 and defined by probability $\delta_{2\%}$. Unlike in the previous case of $\delta_{1,2}$-Al_2O_3, the recursive stacking in $\delta_{2,3,4}$-Al_2O_3 requires that the layers are translationally aligned during stacking and these offsets are included in Table S2.

Model of twinning in θ-Al_2O_3: Twinning in θ-Al_2O_3 can be formulated relatively simply as the recursive stacking of two layers. The two layers are related by mirror symmetry plus translation operations. As shown in Figure 4, the layers were defined in terms of an orthorhombic lattice, with 10 atoms in the layer, which is half the size of conventional θ-Al_2O_3 unit cell.

The rules for recursive stacking are listed in Table S3. The transition from one layer to identical layer corresponds to an un-twinned configuration, while transitions between differing layers corresponds to twinning, with a probability of (twin%).

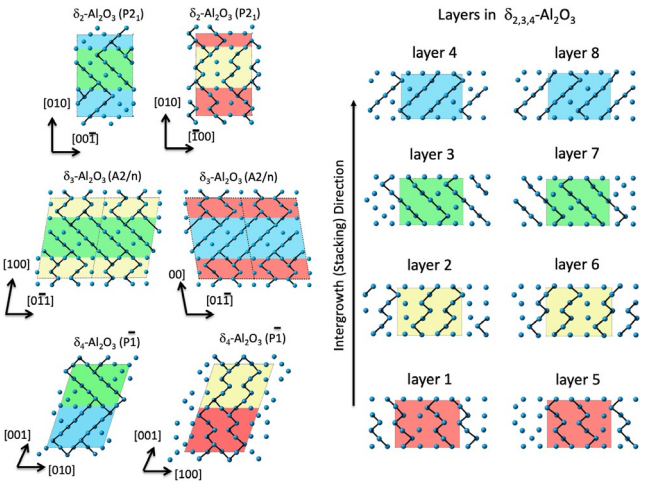

Figure 3. Formulation of structural intergrowth of δ_2-, δ_3- and δ_4-Al_2O_3. The structure is built by eight layers.

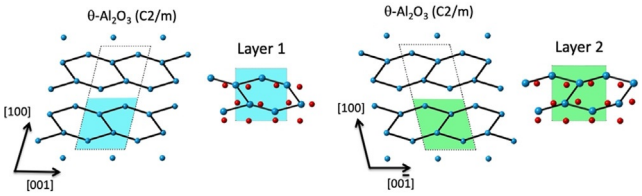

Figure 4. Formulation of twining in θ-Al_2O_3. The twin structure is built by recursive stacking of two layers.

Translational offsets required to accomplish stacking are reported in Table S3.

The Choice of Parameters to Refine

As follows from the description above, the basic structural parameters to represent high temperature transition alumina are the volume fraction of individual intergrowth components V%($\delta_{1,2}$-Al_2O_3), V%($\delta_{2,3,4}$-Al_2O_3) and V%(θ-Al_2O_3), and the level of intergrowth in each component $\delta_{1,2}$-Al_2O_3 ($\delta_{1\%}$,$\delta_{2\%}$), $\delta_{2,3,4}$-Al_2O_3 ($\delta_{2\%}$,$\delta_{3\%}$, $\delta_{4\%}$) and θ-Al_2O_3 (twin%). Additional basic parameters also include lattice parameters of the individual components, crystallite size, atom position within the structures, occupancy, Debye-Waller factor.

The number of potential parameters is consequently relatively large, and determining or refining such a high number of parameters based on the XRD pattern is not likely. To investigate how sensitive XRD is with respect to the different intergrowth/twinning in δ- and θ-Al_2O_3, the individual intergrowth/twinning modes were first evaluated independently in order to understand the effect on diffraction intensities. The simulations were performed using the DIFFAX software package,[16] and a summary for the key intergrowth configurations is shown in Figure 5. In the case of $\delta_{1,2}$-Al_2O_3, we find that changing the relative proportions of δ_1 and δ_2 does not have a significant effect on the main diffraction intensities. Only relatively small differences are observed for diffraction intensities in the low two-theta region, as shown in Figure 5a. Given the expected presence of other components, analysis of intergrowth in $\delta_{1,2}$-Al_2O_3 is not well suited for XRD refinement. In the case of $\delta_{2,3,4}$-Al_2O_3, we find that changing the proportion of intergrowth parts can have a significant effect on the main diffraction intensities. This is especially the case for intergrowth components of δ_2- to δ_3-Al_2O_3. As shown in Figure 5b, increasing the proportion of δ_3-Al_2O_3 within δ_2-Al_2O_3 significantly modifies the relative peak intensities in the range of 30–40° with respect to the diffraction planes in 46–47° range. This is not the case for components $\delta_{2,4}$ Al_2O_3 (Figure 5c), where the intergrowth has only a negligible effect on the diffraction intensities. Analogously to $\delta_{1,2}$-Al_2O_3, only low intensities at relatively low diffraction angles are affected. For θ-Al_2O_3, we find that twinning has a strong effect on the relative intensities, as shown in Figure 5d). Some of the most significant effects are observed for diffraction planes $(40\bar{1})$ and (111), as highlighted with arrows.

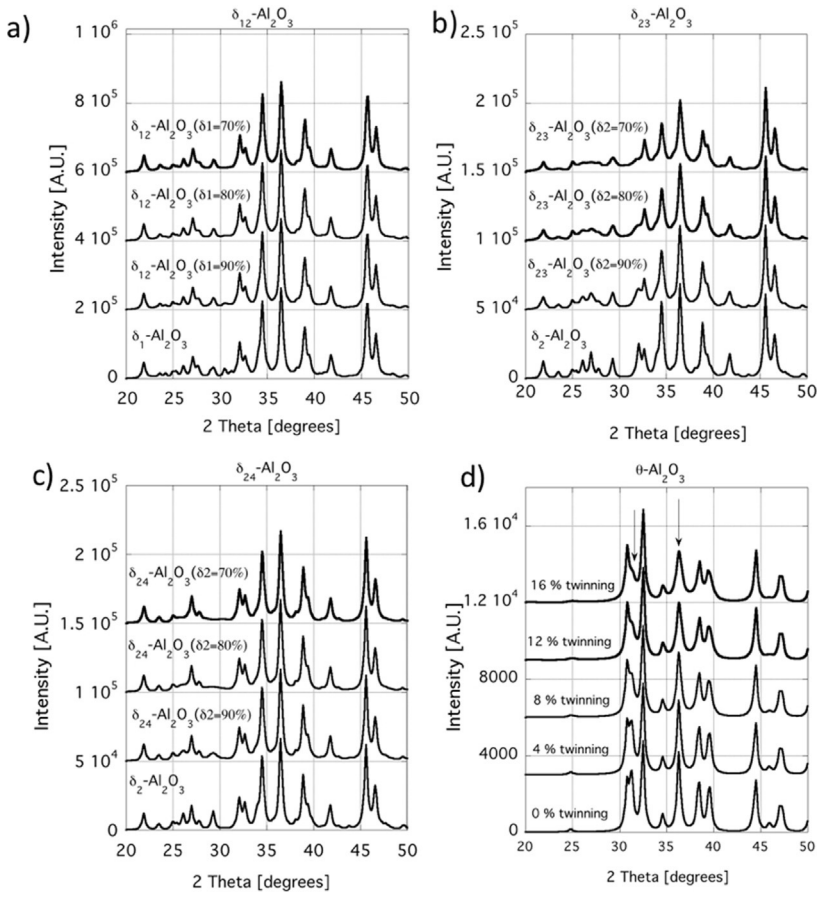

Figure 5. DIFFAX simulated diffraction patterns for the intergrowth structures of a) $\delta_{1,2}$-Al_2O_3, b) $\delta_{2,3}$-Al_2O_3, c) $\delta_{2,4}$-Al_2O_3 and d) twinning in θ-Al_2O_3.

These calculations demonstrate that some intergrowth modes result only in subtle changes in XRD intensities. These are therefore not sensitive to structural refinement using recursive stacking, and this enables us to simplify the parameter space. Since the intergrowth in $\delta_{1,2}$-Al_2O_3 does not have a strong effect on the diffraction intensities, the structure of $\delta_{1,2}$-Al_2O_3 is approximated by δ_1-Al_2O_3. For the structure of $\delta_{2,3,4}$-Al_2O_3, we only consider the contribution from δ_2- and δ_3-Al_2O_3, while omitting δ_4-Al_2O_3. For θ-Al_2O_3, twinning is included as an important intergrowth mode in the refinement.

The summary of structural parameters refined in this work is given in Table 1. The parameters include volume fraction, intergrowth parameters, lattice parameters and crystallite size. Structural parameters that were kept constant include domain size, layers dilation, atomic site positions, site occupancy and Debye-Waller factor. In our work, domain size was considered to be the same as crystallite size, layers dilation to be zero, atomic site positions were derived from DFT methods, site occupancy was considered 1, and Debye-Waller factor of 1.

Tabelle 1: List of structural parameters that were either refined or kept as constant during the refinement.

	$\delta_{1,2}$-Al_2O_3	$\delta_{2,3,4}$-Al_2O_3	θ-Al_2O_3
Volume fraction	YES	YES	YES
Planar disorder model (intergrowth)	NO	ONLY	YES
	δ_1-Al_2O_3	$\delta_{2,3}$-Al_2O_3	twinning
Lattice parameters	YES	YES	YES
Crystallite size	YES	YES	YES
Domain Size	NO	NO	NO
Layers dilatation	NO	NO	NO
Atom positions	NO	NO	NO
Atom occupancy	NO	NO	NO
Debye-Waller factor	NO	NO	NO

Evaluation of the Recursive Stacking Approach

The newly developed recursive stacking approach was tested for its ability to represent the experimental measurements and the ability to well define the intergrowth/twining structural parameters. The tests were performed on samples heat treated at 1050 °C corresponding to different stages of microstructural development.

We find that the recursive stacking formalism provides an important improvement over conventional refinement. An example is shown in Figure 6 for a sample heated for 8 h @1050 °C. Refining the structure using a conventional linear fitting approach resulted in considerable residual intensity, reflected in the merit value, R_{wp}, of 14.8 %. The recursive stacking formalism provided a noticeably better fit to the observed pattern, with smaller residual intensity and R_{wp} of 9.5 %. R_{wp} values around 10 % were typically obtained from

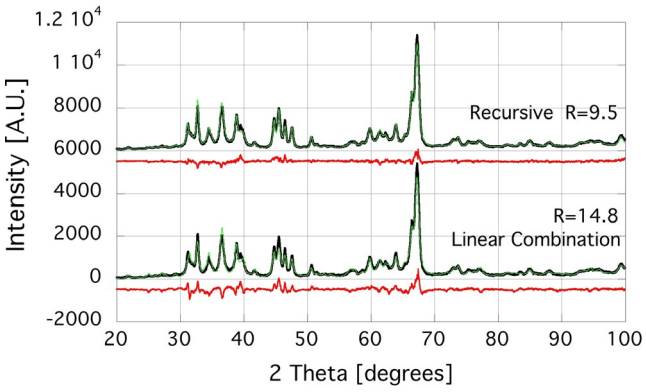

Figure 6. Comparison of XRD refinements based on the recursive formalism and conventional formalism using a linear combination of individual phases. In both cases, the black line represents the experimental observations and the green line represents the refinements. The red line is residual intensity.

refinements of the patterns we investigated. The largest value of 10.7 % was obtained for earliest stages of transformation of 2 h @1050 °C. Although these values are larger than ideal refinements, a larger R_{wp} is expected to originate from not accounting for the presence of small Al sublattice domains in δ-Al_2O_3[14] as well as other microstructural features. Opportunities for improving the modelling of XRD patterns in the early stages of transformation are described in a later section.

The intergrowth in $\delta_{2,3}$-Al_2O_3 and twining in θ-Al_2O_3 parameters are well defined in the search of the best fit of XRD patterns. An example for a sample heat treated for 8 h @1050 °C is shown in Figure 7 a. The merit value (R_{wp}-value) is plotted as a function of the degree of twinning in θ-Al_2O_3 and the fraction of δ_2 in the $\delta_{2,3}$-Al_2O_3, with the global minimum representing the best overall XRD fit. In this particular case we obtained the best fit when $\delta_{2,3}$-Al_2O_3 contained 60 % of δ_2 and θ-Al_2O_3 accommodated 14 % of twinning.

The optimum values cover a relatively narrow range under the tested heat treatment conditions. The uncertainty in identifying the optimum intergrowth/twinning parameter changes slightly as a function of the volume fraction. For example, for longer calcination times, when volume fraction of θ-Al_2O_3 increases to approximately in 60 % and $\delta_{2,3,4}$-Al_2O_3 decreases to 25 %, the definition of twinning improves while the definition of intergrowth parameter slightly worsens, as shown in Figure 7 b. It is likely that this approach may not be well suited for refining the intergrowth/twining parameters if the volume fraction of the component falls below 10 %.

Application to the Quantification of Transition Aluminas

The recursive stacking refinement was applied to study the mechanism and kinetics of phase transformation for samples heated between 2–48 h at 1050 °C. For this time and temperature range, combinations of $\delta_{1,2}$-, $\delta_{2,3,4}$- and θ-Al_2O_3 represent the only possible components of the microstructure. γ-Al_2O_3 can be excluded as the heat treatment extends beyond its stability range, and α-Al_2O_3 formation was not observed.

The derived volume fraction of individual components as a function of calcination time is plotted in Figure 8 a. We find that $\delta_{2,3,4}$-Al_2O_3 is the main component forming in the microstructure in the earliest stages of aging. After 2 hours of aging, it represents approximately 65 % of the total volume fraction. The remaining fraction of the microstructure corresponds to θ-Al_2O_3 rather than $\delta_{1,2}$-Al_2O_3. θ-Al_2O_3 is present at almost 30 % concentration while $\delta_{1,2}$-Al_2O_3 was found only at approximately 5 %. Upon further heat treatment at 1050 °C, $\delta_{2,3,4}$-Al_2O_3 gradually transforms to θ-Al_2O_3 and $\delta_{1,2}$-Al_2O_3, as shown in Figure 8 a. After 48 hrs/1050 °C, the longest time we studied, θ-Al_2O_3 is the main component, at approximately

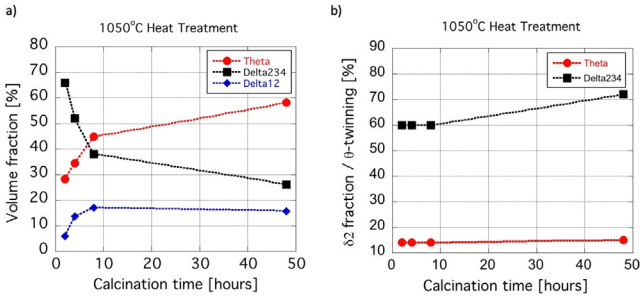

Figure 8. a) Structural evolution of individual components of high temperature transition alumina. b) Evolution of intergrowth disorder in $\delta_{2,3,4}$-Al_2O_3 and twinning in θ-Al_2O_3.

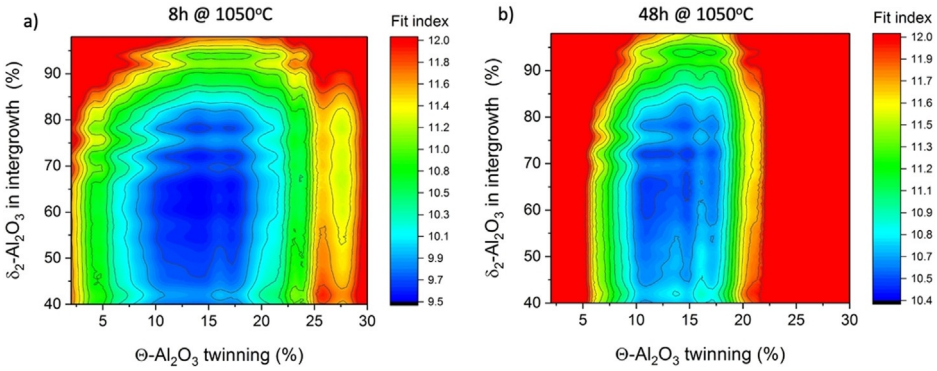

Figure 7. Dependence of Rietveld fit criterion on disorder in $\delta_{2,3}$-Al_2O_3 and θ-Al_2O_3 for sample heat treated a) 8 h at 1050 °C b) 48 h at 1050 °C.

60%, while $\delta_{2,3,4}$-Al_2O_3 decreases to approximately of 25% and $\delta_{1,2}$-Al_2O_3 increases to approximately 15%.

The key take away from these observations is that the two intergrowth modes of δ-Al_2O_3 have very different evolution profiles. The intergrowth of $\delta_{2,3,4}$-Al_2O_3 is predominant in the early stages, while $\delta_{1,2}$-Al_2O_3 is formed from transformation of $\delta_{2,3,4}$-Al_2O_3 with further heat treatment. θ-Al_2O_3 also forms from $\delta_{2,3,4}$-Al_2O_3, but at much higher rate than $\delta_{1,2}$-Al_2O_3. The δ- to θ-Al_2O_3 transformation slows down significantly during the course of heat treatment and after 48 hours the microstructure appears to stabilize in a mixed δ-Al_2O_3/θ-Al_2O_3 state. This finding supports the view that both δ-Al_2O_3 and θ-Al_2O_3 can coexist in a common microstructure over a broad temperature/time range.[10]

During the course of heat treatment, the level of intergrowth in $\delta_{2,3}$-Al_2O_3 or twinning in θ-Al_2O_3 was found to change only to a small degree, as shown Figure 8b. The fraction of δ_2 in the $\delta_{2,3,4}$-Al_2O_3 component increased from approximately 60% for short heating times to 72% after 48 hours. The trend towards a higher fraction of δ_2-Al_2O_3 can be understood on the basis of slightly greater thermodynamic stability for δ_2, and also based on the fact that δ_3-Al_2O_3 can readily transform to θ-Al_2O_3 due to symmetry similarities.[10] For the structure of θ-Al_2O_3, we find that the degree of twinning stays approximately constant throughout the course of transformation, corresponding to ≈14%.

As a part of the structural refinement, we also evaluated the lattice parameters of $\delta_{1,2}$-, $\delta_{2,3,4}$- and θ-Al_2O_3. As shown in Figure 9, we find that the lattice parameters show little variation, and stay mostly within the range of experimental errors during the course of heat treatment. One of few exceptions is the lattice parameter for [100] of θ-Al_2O_3, which is found to continuously evolve towards lower values during the course of heat treatment with a total change of 0.25%. Evolution towards smaller [100] lattice parameters would be expected under the circumstances that θ-Al_2O_3 changes towards a smaller amount of 2D disorder. We note that the change of 2D disorder should be also associated with an expansion of [010], but this is observed only partially. As such, judging the nature of disorder in θ-Al_2O_3 from lattice parameters is an intriguing prospect but its applicability should be investigated further. In microstructures containing δ-Al_2O_3/θ-Al_2O_3 boundaries, the variation in lattice parameters is also expected to be governed by coherency strains, and this may limit the utility of the approach.

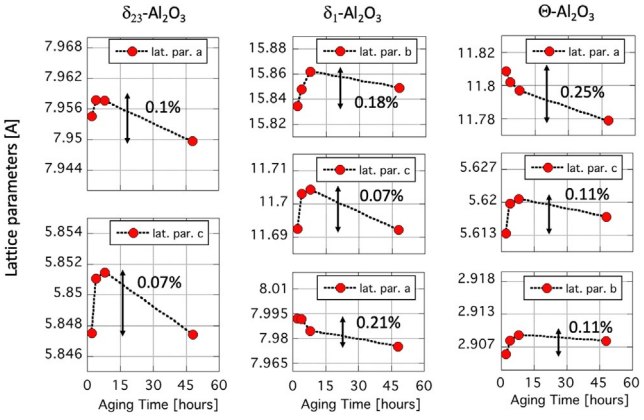

Figure 9. Lattice parameters from XRD recursive refinements as a function of time at 1050°C. The lattice parameters for $\delta_{2,3,4}$-Al_2O_3 are given in terms of the basic intergrowth unit. For $\delta_{1,2}$-Al_2O_3, the lattice parameters are given in terms of orthorhombic $P2_12_12_1$ ($a \approx a_\gamma$, $b \approx 2a_\gamma$, $c \approx 1.5a_\gamma$). For θ-Al_2O_3, the lattice parameters are represented in terms of the monoclinic C2/m crystal.

Discussion

The current work demonstrates that explicitly accounting for planar disorder in δ-Al_2O_3 and θ-Al_2O_3 is necessary to model XRD patterns of high temperature transition alumina. By accounting for the planar disorder, it is possible to derive volume fractions for individual components and their level of intergrowth/twinning, which represent the key structural parameters for understanding the mechanism of phase transformations. However, the planar disorder is not the sole type of disorder found in the microstructure of high temperature aluminas. Other types of disorder are present, especially in the earlier stages of microstructure transformation. This is evident from higher values of R, which show that the planar disorder alone cannot fully represent the experimentally obtained XRD patterns.

An important structural parameter, which has not been accounted for in the present work, is the size of δ-Al_2O_3 and θ-Al_2O_3 domains. In the context of transition aluminas, the domains are differentiated from the crystallites. Domains represent a discontinuity of the Al sublattice but with the oxygen sublattice being continuous, as schematically shown in Figure 10a. Physically, the discontinuity in Al sublattice can be explained by the presence of rotationally and translationally related variants of δ- and θ-Al_2O_3 sharing a common oxygen sublattice.[14] Accounting for the domains is expected to be important, especially in the early stages of δ-Al_2O_3 formation when the microstructure can accommodate a high density of Al domains with size well below ≈10 nm.[14] The presence of domains can be modeled using the Debye scattering equation,[21] which explicitly includes every atom

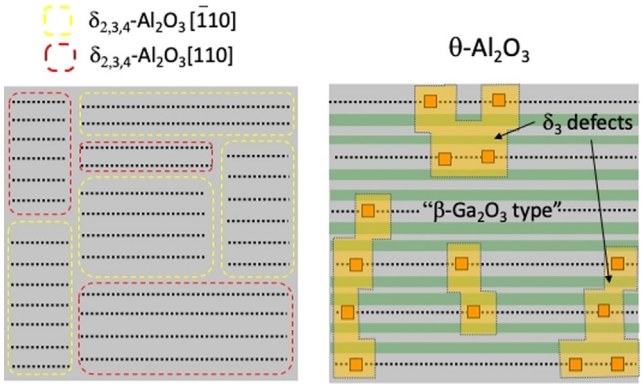

Figure 10. a) Schematic of domain microstructure of δ-Al_2O_3 in the earlier stage of formation. b) Schematic of 2D disorder in θ-Al_2O_3. „β-Ga_2O_3" structure type can accommodate δ_3-Al_2O_3 bonding environment.

in the structure rather than applying a periodic repeat. This approach has been previously applied to study the faulted structure of γ-Al_2O_3 in the work of Pakharukova et al.[7]

Another structural parameter that should be considered in the future work is the 2D disorder in θ-Al_2O_3. The disorder arises from reordering of subset of octahedral and tetrahedral sites, as they change from „β-Ga_2O_3" to δ_3-Al_2O_3 bonding environment, as schematically shown in Figure 10b. The disorder is non-periodic and can be modeled using Debye scattering equation using a superstructure. It is noted that refinement against observed data can become computationally expensive using Debye scattering equation, and a possible alternative approach is to approximate the disorder using partial occupancies in conventional cell. Partial occupancy for oxygen and Al sites were previously shown to improve fit for θ-Al_2O_3.[9] Provided that a correlation can be established, the use of partial occupancies could provide a non-physical but a valuable alternative for easy estimation of disorder in θ-Al_2O_3.

The high number of parameters needed to represent the microstructure of high-temperature transition aluminas raises a question whether XRD alone can be used for their determination. Individually, the parameters may converge robustly but refining the large number of parameters all together may not lead to a unique solution. In addition, XRD also has a poor sensitivity to address some disorder types, such as the intergrowth of $\delta_{1,2}$-Al_2O_3 and δ_4 in $\delta_{2,3,4}$-Al_2O_3, as demonstrated by DIFFAX simulations. Consequently, it can be reasoned that the quantification of transition alumina may require the use of complementary techniques, ideally under global refinement. In this respect, the complementary use of NMR is especially attractive as it provides an independent quantification of octahedral and tetrahedral sites, and a valuable information about the local bonding environment of Al due to the sensitivity of quadrupole nuclear magnetic moment of ^{27}Al.[22,23]

Complementary use of NMR and XRD has been previously applied for quantification of 2D disorder in θ-Al_2O_3 when θ-Al_2O_3 is accommodated in a common microstructure with δ-Al_2O_3.[10] For θ-Al_2O_3 alone, the analysis could be accomplished without the use of XRD since the amount of 2D disorder could be directly linked to the ratio of octahedral/tetrahedral sites. However, in δ-Al_2O_3/θ-Al_2O_3 microstructure, the knowledge of volume fractions, as determined from XRD, is required. In the previous work,[10] the XRD quantification utilized a simplified model for θ-Al_2O_3 without the 2D disorder. Provided that 2D disorder can implemented for XRD pattern modelling, it can be envisioned that the derivation of both 2D disorder and volume fraction can be done in a combined XRD-NMR iterative fashion for improved accuracy and reliability.

It is noted that a key assumption in the combined analysis presented by Kovarik et al.[10] is that δ-Al_2O_3 contain a known percentage of 37.5% of tetrahedral sites. However, in the earlier stages of transformations, when δ-Al_2O_3 undergoes development, this assumption may not be justified. The need to consider a lower percentage of tetrahedral sites in the earlies stages is shown in Figure 11a, which plots the overall fraction of tetrahedral sites in the microstructures as a function of volume fraction of δ-Al_2O_3/θ-Al_2O_3 for samples heated at 1050°C. At 2 hours of aging, the overall fraction of tetrahedral sites is found to be $\approx$38%. Given that fact that the microculture contain 70% of δ-Al_2O_3 (as derived with XRD), and assuming 37.5% of tetrahedral sites, then the corresponding number of tetrahedral sites in 30% of θ-Al_2O_3 would have to drop to unrealistically low value of 39%. Instead, it is more realistic to consider that δ-Al_2O_3 accommodates a smaller fraction of tetrahedral sites in the earlier stage, as documented with a plausible range in Figure 11a, which would then increase the tetrahedral sites in θ-Al_2O_3. The physical origin for the modification of tetrahedral/octahedral ratio in δ-Al_2O_3 is not known, but the presence of defects, such as porosity (surfaces with modified Al_{Oh}/Al_{Td}), domain boundaries, or point defects can be hypothesized as the origin.

Quantification of the different transition alumina phases can be also pursued on the basis of NMR chemical shift and line shape analysis.[22,23] The non-spherical charge distribution around the ^{27}Al nucleus gives rise to a quadrupole moment, which results in signal broadening which, when coupled with sites at similar spectral positions greatly complicates quantification of ^{27}Al species in mixtures of transition alumina phases. However, the unique chemical shifts and line shape parameters which reflect the differences in the local bonding

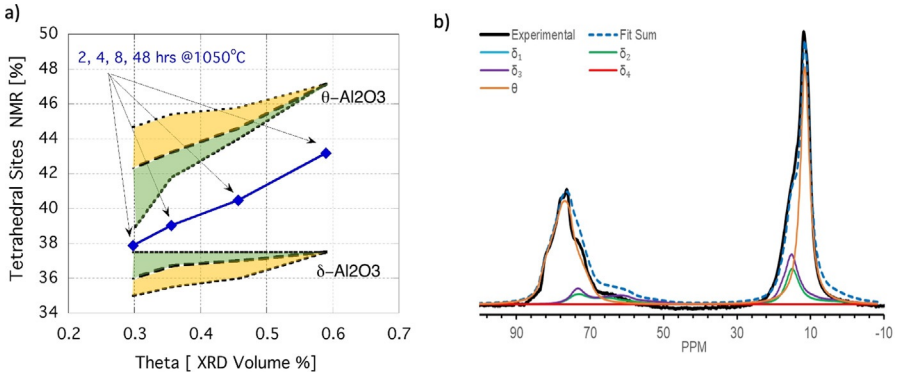

Figure 11. a) NMR determination of the tetrahedral and octahedral sites within the structure of transition Aluminas. b) NMR spectra of a sample heated for 48 hours at 1050°C represented as a linear combination of δ_2, $\delta_3$and θ-Al_2O_3. (Lorentzian 600 Hz line broadening).

environment of alumina species can be exploited for rigorous quantification if they are known precisely. Given that both δ- and θ-Al_2O_3 contain numerous octahedral and tetrahedral sites (e.g. 10 crystallographically distinct octahedral sites for δ_1-Al_2O_3 alone) and the proportion of the components changes with heat treatment conditions, NMR spectra for δ- and θ-Al_2O_3 should not be considered as comprising one tetrahedral and one octahedral resonance for each phase. One approach to address this quantification challenge is to use DFT-based electronic calculations of the ^{27}Al nuclei to simulate the line profiles for individual δ_1-Al_2O_3, δ_2-Al_2O_3, δ_3-Al_2O_3, δ_4-Al_2O_3, and θ-Al_2O_3 components as a basis for simulation. In Figure 11b, we show NMR spectra previously published in our work[10] and a corresponding deconvolution fit represented as a linear combination of DFT-calculated δ_1, δ_2, δ_3, δ_4, and θ-Al_2O_3 (β-Ga_2O_3 structure) NMR profiles. The best fit was obtained for a composition comprised of $\delta_2 = 13\%$, $\delta_3 = 19.4\%$ and θ-$Al_2O_3 = 67.6\%$. The fraction of δ-Al_2O_3/θ-Al_2O_3 is fairly consistent with XRD results (Figure 8) while the fraction of individual components of δ_x-Al_2O_3 differs. We note that the fit quality and corresponding composition are highly sensitive to the line-broadening applied to the DFT simulations; however, the general ability to represent NMR spectra in this fashion is encouraging for future quantification. Further work on combing NMR and XRD methods for comprehensive quantification of high temperature transition aluminas is ongoing.

In addition to NMR and XRD, there are a number of other techniques that can provide further constraints for the structure of these complex materials. It can be envisioned that multimodal approaches, ideally used under global refinement, will allow for better quantification of these complex materials. Such approaches can include other techniques such as skeletal Raman spectroscopy, PDF or Neutron diffractions that have shown to provide valuable information about transition aluminas.[15,24,25]

Conclusion

The current work demonstrates the utility of a recursive stacking formalism for quantification of high temperature transition aluminas in the δ-Al_2O_3/θ-Al_2O_3 stability range. We find that a recursive stacking approach allows quantification of the intergrowth types of δ-Al_2O_3 and θ-Al_2O_3, and its application provides a significant improvement to the fit of experimental data. The newly developed XRD refinement was applied to study the mechanism of transformation δ-Al_2O_3 to θ-Al_2O_3. It was shown that different intergrowth modes in δ-Al_2O_3 undergo different transformation pathways, and that a significant fraction of δ-Al_2O_3 remains stabilized even after prolonged exposures to high temperatures. Even with the improvements, we find limitations to quantification using the recursive stacking approach and have outlined future directions for possible multimodal XRD and NMR analysis of transition aluminas.

Acknowledgements

This work was performed in the Wiley Environmental Molecular Sciences Laboratory (EMSL), a national scientific user facility sponsored by DOE's Office of Biological and Environmental Research and located at PNNL. The work was supported by the U.S. Department of Energy (DOE), Office of Basic Energy Sciences, Division of Chemical Sciences, Geosciences, and Biosciences.

Conflict of interest

The authors declare no conflict of interest.

Stichwörter: alumina · phase transformations · quantification of disorder · transition aluminas · XRD recursive stacking

[1] G. Busca, *Catal. Today* **2013**, *226*, 1 – 12.
[2] R. Wischert, P. Laurent, C. Copéret, F. Delbecq, P. Sautet, *J. Am. Chem. Soc.* **2012**, *134*, 14430 – 14449.
[3] M. Trueba, S. Trasatti, *Eur. J. Inorg. Chem.* **2005**, 3393 – 3403.
[4] I. Levin, D. Brandon, *J. Am. Ceram. Soc.* **1998**, *81*, 1995 – 2012.
[5] M. Digne, P. Sautet, P. Raybaud, P. Euzen, H. Toulhoat, *J. Catal.* **2004**, *226*, 54 – 68.
[6] L. Kovarik, A. Genc, C. Wang, A. Qiu, C. H. Peden, J. Szanyi, J. H. Kwak, *J. Phys. Chem. C* **2013**, *117*, 179 – 186.
[7] V. P. Pakharukova, D. A. Yatsenko, E. Y. Gerasimov, A. S. Shalygin, O. N. Martyanov, S. V. Tsybulya, *J. Solid State Chem.* **2017**, *246*, 284 – 292.
[8] S. J. Wilson, *J. Solid State Chem.* **1979**, *30*, 247 – 255.
[9] R.-S. Zhou, R. L. Snyder, *Acta Crystallogr. Sect. B* **1991**, *47*, 617 – 630.
[10] L. Kovarik, M. Bowden, D. Shi, N. M. Washton, A. Andersen, J. Z. Hu, J. Lee, J. Szanyi, J. H. Kwak, C. H. F. Peden, *Chem. Mater.* **2015**, *27*, 7042 – 7049.
[11] J. Lee, H. Jeon, D. G. Oh, J. Szanyi, J. H. Kwak, *Appl. Catal. A* **2015**, *500*, 58 – 68.
[12] G. Busca, *Adv. Catal.* **2014**, *57*, 319 – 404.
[13] L. Kovarik, M. Bowden, A. Genc, J. Szanyi, C. H. F. Peden, J. H. Kwak, *J. Phys. Chem. C* **2014**, *118*, 18051 – 18058.
[14] L. Kovarik, M. Bowden, D. Shi, J. Szanyi, C. H. F. Peden, *J. Phys. Chem. C* **2019**, *123*, 9454 – 9460.
[15] G. Paglia, E. S. Božin, S. J. L. Billinge, *Chem. Mater.* **2006**, *18*, 3242 – 3248.
[16] M. Treacy, J. M. Newsam, M. W. Deem, *Proc. R. Soc. London Ser. A* **1991**, *433*, 499 – 520.
[17] T. Willhammar, X. Zou, *Z. Kristallogr. - Cryst. Mater.* **2013**, *228*, 11 – 27.
[18] J.-R. Hill, C. M. Freeman, M. H. Rossouw, *J. Solid State Chem.* **2004**, *177*, 165 – 175.
[19] R. F. Giese, Jr., R. Snyder, V. A. Drits, A. S. Bookin, *Clays Clay Miner.* **1989**, *37*, 203 – 210.
[20] Y. Wang, P. Bronsveld, J. De Hosson, B. Djuricic, D. McGarry, S. Pickering, *J. Eur. Ceram. Soc.* **1998**, *18*, 299 – 304.
[21] A. Leonardi, D. L. Bish, *J. Appl. Crystallogr.* **2016**, *49*, 1593 – 1608.
[22] C. V. Chandran, C. E. A. Kirschhock, S. Radhakrishnan, F. Taulelle, J. A. Martens, E. Breynaert, *Chem. Soc. Rev.* **2019**, *48*, 134 – 156.

[23] L. A. O'Dell, S. L. P. Savin, A. V. Chadwick, M. E. Smith, *Solid State Nucl. Magn. Reson.* **2007**, *31*, 169 – 173.
[24] G. Paglia, C. Buckley, A. Rohl, B. Hunter, R. Hart, J. Hanna, L. Byrne, *Phys. Rev. B* **2003**, *68*, 144110.
[25] H.-S. Kim, P. C. Stair, *J. Phys. Chem. A* **2009**, *113*, 4346 – 4355.

Manuskript erhalten: 10. Juli 2020
Akzeptierte Fassung online: 20. August 2020
Endgültige Fassung online: 23. September 2020

